An Automatic Phase-Change Detection Technique for Colloidal Hard Sphere Suspensions

Mark McDowell
Glenn Research Center, Cleveland, Ohio

Elizabeth Gray
Scientific Consulting, Inc., Cleveland, Ohio

Richard B. Rogers
Glenn Research Center, Cleveland, Ohio

The NASA STI Program Office . . . in Profile

Since its founding, NASA has been dedicated to the advancement of aeronautics and space science. The NASA Scientific and Technical Information (STI) Program Office plays a key part in helping NASA maintain this important role.

The NASA STI Program Office is operated by Langley Research Center, the Lead Center for NASA's scientific and technical information. The NASA STI Program Office provides access to the NASA STI Database, the largest collection of aeronautical and space science STI in the world. The Program Office is also NASA's institutional mechanism for disseminating the results of its research and development activities. These results are published by NASA in the NASA STI Report Series, which includes the following report types:

- TECHNICAL PUBLICATION. Reports of completed research or a major significant phase of research that present the results of NASA programs and include extensive data or theoretical analysis. Includes compilations of significant scientific and technical data and information deemed to be of continuing reference value. NASA's counterpart of peer-reviewed formal professional papers but has less stringent limitations on manuscript length and extent of graphic presentations.

- TECHNICAL MEMORANDUM. Scientific and technical findings that are preliminary or of specialized interest, e.g., quick release reports, working papers, and bibliographies that contain minimal annotation. Does not contain extensive analysis.

- CONTRACTOR REPORT. Scientific and technical findings by NASA-sponsored contractors and grantees.

- CONFERENCE PUBLICATION. Collected papers from scientific and technical conferences, symposia, seminars, or other meetings sponsored or cosponsored by NASA.

- SPECIAL PUBLICATION. Scientific, technical, or historical information from NASA programs, projects, and missions, often concerned with subjects having substantial public interest.

- TECHNICAL TRANSLATION. English-language translations of foreign scientific and technical material pertinent to NASA's mission.

Specialized services that complement the STI Program Office's diverse offerings include creating custom thesauri, building customized databases, organizing and publishing research results . . . even providing videos.

For more information about the NASA STI Program Office, see the following:

- Access the NASA STI Program Home Page at *http://www.sti.nasa.gov*

- E-mail your question via the Internet to help@sti.nasa.gov

- Fax your question to the NASA Access Help Desk at 301–621–0134

- Telephone the NASA Access Help Desk at 301–621–0390

- Write to:
  NASA Access Help Desk
  NASA Center for AeroSpace Information
  7121 Standard Drive
  Hanover, MD 21076

NASA/TM—2005-213989

An Automatic Phase-Change Detection
Technique for Colloidal Hard
Sphere Suspensions

Mark McDowell
Glenn Research Center, Cleveland, Ohio

Elizabeth Gray
Scientific Consulting, Inc., Cleveland, Ohio

Richard B. Rogers
Glenn Research Center, Cleveland, Ohio

National Aeronautics and
Space Administration

Glenn Research Center

October 2005

Acknowledgments

An Automatic Phase-Change Detection Technique
for Colloidal Hard Sphere Suspensions

Mark McDowell
National Aeronautics and Space Administration
Glenn Research Center
Cleveland, Ohio 44135

Elizabeth Gray
Scientific Consulting, Inc.
Cleveland, Ohio 44135

Richard B. Rogers
National Aeronautics and Space Administration
Glenn Research Center
Cleveland, Ohio 44135

Abstract

Colloidal suspensions of monodisperse spheres are used as physical models of thermodynamic phase transitions and as precursors to photonic band gap materials. However, current image analysis techniques are not able to distinguish between densely packed phases within conventional microscope images, which are mainly characterized by degrees of randomness or order with similar grayscale value properties. Current techniques for identifying the phase boundaries involve manually identifying the phase transitions, which is very tedious and time consuming. We have developed an intelligent machine vision technique that automatically identifies colloidal phase boundaries. The algorithm utilizes intelligent image processing techniques that accurately identify and track phase changes vertically or horizontally for a sequence of colloidal hard sphere suspension images. This technique is readily adaptable to any imaging application where regions of interest are distinguished from the background by differing patterns of motion over time.

Introduction

Colloidal suspensions of uniformly sized spheres undergo a disorder-order phase transition under certain conditions. Such monodisperse suspensions are useful as a physical model of thermodynamic phase transitions in conventional engineering materials (Pusey, 1986), (Grier and Murray, 1994), (Elliot et al., 1997), (Gasser et al., 2001) and as precursors to photonic band gap materials (Bogomolov et al., 1997), (Wijnhoven and Vos, 1998), (Zakhifov et al., 1998), (Subramania et al., 1999). We desire to study several aspects of a moving colloidal liquid-colloidal solid interface using conventional optical microscopy. This paper describes an approach to automatically track the position and shape of this solid-liquid interface.

Our experiments are the colloidal equivalent of directional solidification techniques in conventional materials processing. We use suspensions which closely approximate a hard sphere potential where thermodynamic phase behavior is solely a function of volume fraction φ, which is the proportion of total volume occupied by particles. Below the freezing volume fraction, $\varphi_f = 0.494$, spheres are disordered and free to diffuse throughout the entire sample. Above the melting volume fraction, $\varphi_m = 0.545$, a sample becomes crystalline where each particle is "caged" by its neighbors and restricted to movement about a lattice point. Between φ_f and φ_m is a regime of coexisting colloidal liquid and colloidal crystal (Pusey, 1986). In our experiments, we begin with suspensions prepared well below φ_f and allow either

slow evaporation or gravitational sedimentation to concentrate the spheres to one end of a cell where crystallization occurs.

When the sphere size falls within a range accessible to optical microscopy, disordered (or "liquid") phases and ordered (or "solid") phases are clearly visible in the colloidal system.

The scientific data of interest is extracted from the area of the colloidal sample around the solid/liquid interface. Therefore, it is necessary to keep this interface in the microscope's field of view as it grows. Typical interface velocities are on the order of a few microns per hour. Since a single experiment can last from days to weeks, it is impractical to require human intervention to ensure that the front remains in the microscope's field of view. Instead, it would be preferable to automatically track the disorder/order phase front for a colloidal hard sphere system. We accomplish this by implementing an image processing algorithm that is based on the difference between the time-averaged particle behaviors of the two phases. This difference in particle behavior leads to differing grayscale levels for the two phases in images averaged over appropriate time intervals. We exploit this difference in order to extract the phase boundary.

Most current image processing algorithms track particles by distinguishing them from a background. The challenge here is that the spheres are too densely packed for these conventional approaches. The volume fractions of the colloidal solid and colloidal liquid at the phase interface are φ_m and φ_f, respectively. This corresponds to particle separations near the interface that are on the order of 1/10 of a particle diameter. In addition, the microscope depth of field is comparable to the particle diameter, so particles above and below an ideal focal plane also contribute to most images. This results in images with touching or overlapping spheres without even a single pixel to separate them. There is no "background". Typical tracking algorithms based on foreground/background intensity differences will not suffice. The phases only differ in the ordering of the particles, which adds another level of complexity to the problem.

Furthermore, constant illumination by the microscope would cause unwanted thermal gradients. The solution must include a means of automatically controlling the microscope to not only move the stage and acquire images as the disorder/order phase front grows, but also to control the lamp intensity.

Some researchers have differentiated colloidal phases by post-processing video data to extract the centroid of each particle and then calculating bond orientation order parameters (Grier and Murray, 1994), (Gasser et al., 2001). However, this approach is computationally intensive and not feasible for real-time control of the microscope. Furthermore, this method is difficult to apply to hard sphere systems because centroid extraction typically requires the use of dyed particles and confocal microscopy, and it had been found that the dye tends to soften the interparticle potential (Gasser et al., 2001). In contrast, our approach can be used with hard sphere particles using conventional microscopy techniques and undyed spheres, and the necessary processing steps can be performed quickly enough to be used for stage control purposes.

Materials and Methods

Before our technique was developed, the optimal way to detect the interface in a colloidal hard sphere experiment was to have a person use an image digitizer and trace the contour of the interface manually, which is extremely time consuming and is prohibitively expensive due to the large number of images that represent a typical colloid experiment. A typical experiment can consist of hundreds to thousands of images. Consequently, we have developed, tested and implemented a technique that will accurately detect the interface of colloidal hard sphere experiments automatically and continually over long time periods without human intervention. What follows is a brief overview of our experimental procedure and an explanation of our interface detection technique.

Experimental Setup and Image Acquisition

The colloidal particles were 1.1 µm diameter poly (methyl methacrylate) (PMMA) spheres with a grafted layer of poly (12-hydroxy stearic acid) (PHSA) chains. These spheres were dispersed in a

combination of organic solvents, decalin, and tetralin, to closely match the sphere and fluid indices of refraction in order to avoid sample turbidity at the high volume fractions of interest. Such suspensions have been shown to closely follow the hard sphere equation of state (Phan et al., 1996). Comparison with test particles embedded in optical epoxy of known index of refraction suggests that Δn/n<0.01 for our suspensions. Since particle separation increases as the interparticle potential is "softened" from the hard sphere potential, experiments with hard spheres represents the most challenging image processing scenario for phase interface detection.

The experimental cell was constructed by placing a measured drop of suspension between a standard microscope slide and coverslip and sealing the edges with epoxy. This produced a test section that was ~25 μm thick. A slow evaporation from one side of the cell resulted in a volume fraction gradient which produced a moving solid/liquid interface. This served as a precursor experiment to ongoing work using the more controlled conditions of gravitational settling. We used an upright biological microscope with a 63x/1.3NA objective in the transmitted light differential interference contrast (DIC) mode. We have also been successful in applying this technique using phase contrast optics. Though the Rayleigh criterion would suggest a resolution limit of about 1/4 μm at this numerical aperture, we find that practical imaging with such closely index-matched particles is limited to particle diameters of about 1/2 μm and larger. Images were acquired from the center of the cell volume at the solid/liquid interface using a CCD camera and recorded on videotape at 30 frames per second. Following the experiment, sequential images were acquired from the videotape and stored as individual files for processing.

Detecting the Colloid Interface

The colloidal system consists of two phases, a solid or ordered phase and a liquid or disordered phase. These two phases are separated by a narrow transitional region predicted by theory to be about 3 to 7 particle diameters wide for systems with a hard sphere potential (Curtain, 1989; Chowhury, and Ghosh, 1998). Our technique locates the interface between ordered ("solid") and disordered ("liquid") regions in a colloidal suspension. The technique uses frame averaging, brightness slicing, filtering, and a particle finding algorithm on a series of image files. The orientation of the growing crystal is left to right (figure 1 vertical interface) where the colloidal liquid occupies the rightmost 1/4 of the image while the colloidal solid occupies the leftmost 3/4. Four different crystal grains lie along the solid side of the interface, and each grain has a different crystallographic orientation, as deduced by human visual inspection.

Frame averaging

The core of our interface detection technique is based on the fundamental difference between the behavior of individual spheres in colloidal liquid and the colloidal solid phases. In the liquid phase, the spheres are not localized. Rather, there is sufficient room for them to diffuse freely throughout the liquid phase. In contrast, spheres in the solid phase are arranged in 3-D crystalline order, and the spacing between particles is so small that movement is limited almost exclusively to a small "cage" defined by nearest neighbors. This allows us to use frame averaging to separate solid from liquid. When a number of frames are averaged, the liquid portion tends to become blurred or grayed out while the solid portion maintains or increases its clarity and contrast.

The time scale of the image sequence for frame averaging is set by the characteristic time scale of the particle motion. This can be determined by calculating the average time required for a particle to diffuse its radius, α (Poon, 1995). The mean square displacement of a colloidal particle, E^2, is given by the Einstein-Smoluchowski equation:

$$E^2 = 6D\tau \tag{1}$$

where τ is the time duration considered and D is the diffusion coefficient given by the Stokes-Einstein relation,

$$D = \frac{k_B T}{6\pi a \eta} \qquad (2)$$

where k_B is Boltzmann's constant, T is the absolute temperature and η is the viscosity of the suspending liquid. By combining equations (1) and (2) and using the square of the particle radius for E^2, the time to diffuse a particle radius, τ_a, is

$$\tau_\alpha = \frac{\pi \eta a^3}{k_B T} \qquad (3)$$

For our colloidal suspension, $\tau_a = 0.3$s. We expect that our technique will require time intervals equal to or greater than τ_a.

Frame averaging was performed by summing the values at a pixel location over a series of frames and dividing by the number of frames. Equation (4) gives the output pixel value at row i, column j based on a series of n input images.

$$O_{ij} = \frac{\sum_n I_{ij}}{n} \qquad (4)$$

i,j: row and column position of the pixel in a frame (image)
n: number of frames
I: input pixel
O: output pixel

Figures 1 and 2 give an example of a typical image and the averaged image over a series of frames. Note the loss of contrast in the liquid portion of the averaged image.

Brightness slicing

The brightness slicing technique is used to create a high-contrast image that specifically highlights a particular object of interest and works well in separating objects that have either light or dark values from a background with intermediate values. Brightness slicing is performed utilizing user-defined threshold values. The technique is performed on a series of frame-averaged images and when applied, the result will be a solid region highlighted in white against a black background, thereby making the solid-liquid interface location easy to determine.

More specifically, brightness slicing is a double binary contrast enhancement operation where user-defined pixel intensity values below a lower threshold and above an upper threshold are set to white, while values between the two thresholds are set to black. Ideally, the liquid or blurry region is set to black while the solid region is set to white. Equation (5) gives the formula for determining the output pixel value at row i, column j given the user-defined upper and lower threshold values.

$$O_{ij} = 0, \; \alpha_1 \le I_{ij} \le \alpha_2 \qquad (5)$$
$$= 1, \text{ otherwise}$$

α_1: lower threshold value
α_2: upper threshold value

This operation refines the averaging operation by further differentiating liquid from solid regions with the result being a mostly white solid region and a mostly black liquid region. Because the solid region contains some of the same intensity values as the liquid regions, some erosion of the particles may occur.

Figure 3 illustrates a typical colloid image after utilizing our brightness slicing technique. Notice there is now a distinctive separation pattern between the solid and liquid regions of the image (McDowell, 2003).

Clean technique

This technique cleans the image using a center-deleted spike filter modified to remove noise not associated with particles. It is designed to work on images that consist of light particles on a black background and is described by (Crouser, Bethea, and Merat, 1997). The clean filter works by summing the pixel values surrounding a central pixel of interest. The center pixel is not included in the sum. If the sum is less than an adjustable clutter threshold, the area is determined to be background clutter (i.e., not in the vicinity of a particle) and the pixel of interest is set to 0. The pixel value is unchanged if the sum is greater than or equal to the clutter threshold. Two additional parameters are present, the filter size and the significance threshold. The filter size designates the extent of the neighborhood around the current pixel that will determine its output value. The significance threshold is a way to disregard low level noise. Pixels with a grayscale value less than the significance threshold are not included in the sum. The clean filter is an effective method for cleaning up background and spike noise while not attenuating particles.

Mathematically this is defined as:

$$r(i,j) \quad = \quad \Sigma\Sigma f(k,l) * g(i+k, j+l) * H(g(i+k, j+l) - \lambda_1) \tag{6}$$

where: k,l are elements of $\{-1,0,1\}$ for a 3 by 3 filter

$$h(i,j) \quad = \quad g(i,j) * H(r(i,j) - \lambda_2) \tag{7}$$

where

$$
\begin{aligned}
H(x) \quad &= \quad 0 \text{ if } x < 0 \\
&= \quad 1 \text{ otherwise}
\end{aligned} \tag{8}
$$

$g(x,y)$ = the grayscale pixel value of the pixel located at (x,y)

$f(k,l)$ = the filter kernel value at (k,l) (0 at $k = 0$, $l = 0$, 1 everywhere else)

$r(i,j)$ = the output of the convolution step

$h(i,j)$ = the output of the filtering operation = the new value of the pixel at (i,j)

λ_1 = a significance threshold for each pixel in the summation (significance Threshold)

λ_2 = the output threshold for the filter (clutter Threshold)

Applying the clean technique after the brightness slice operation greatly attenuates the noise in the liquid region while leaving the solid region largely unchanged (fig. 4). Note that the processing techniques have worked equally well for each of the four crystallographic orientations represented along the interface.

Image dilation technique

After the brightness slice and clean operations, the solid portion of the image is made up of many individual white pixels. The "find particles" technique will only find particles that are 8-connected. An 8-connected object has a continuous perimeter that can be traced by traveling in 8 directions (up, down, left,

right, and diagonals) and at least one pixel separating the object from the image edge. It is necessary to dilate the white pixels to ensure that they will form a connected mass. For this experiment, the best dilation technique was a 7 by 7 low pass filter with zero at the center and larger weights away from the center (fig. 6).

The low pass filter is applied to the cleaned image resulting in dilation of the individual white particles to form a solid mass (fig. 7). After the dilation operation, a thin strip along the borders of the image is blacked out to ensure the solid region will be separated from the image edge.

Find particles technique

After image dilation, a find particles algorithm described by (Bethea, 1996) is applied. This technique scans an image and identifies every non-background object. This function searches a grayscale image for non-background particles using an eight directional search (N, NE, E, SE, S, SW, W, and NW) and looks for the largest non-background particle in the image, which represents the transition mapping of the solid/liquid interface.

Figure 7 shows the result of the find particles algorithm. Notice the algorithm found one very large particle representing the entire solid region. The particle perimeter is identified and the particle number (1) is drawn at the intensity-weighted center of mass of the particle.

Interface determination

The largest particle found is determined to be the solid region. Depending on the orientation of the sample, the topmost pixel in each column or the rightmost pixel in each row is taken as the solid/liquid interface. The automated interface solution is superimposed on the original unprocessed image with a contrast line as shown in figure 8. The data from this line is stored in a database and associated with the corresponding image file.

Results

In order to verify the accuracy and reliability of the interface detection technique, we conducted three separate analyses of a sequence of images taken from a colloid hard sphere experiment. We chose a subset of 10 images with a 0.33 second time interval between each image. This time interval was slightly greater than τ_a for our colloidal system. In line with expectation, our technique did not work properly for time intervals less than τ_a. The average velocity of the interface for this experiment was 2.6 microns/hr. Therefore, in 0.33 seconds, the net growth of the interface would only be about 1/4 nm, which is essentially a stationary interface over the duration of the image sequence. Figure 9 shows an example of the first, fifth, and tenth image in the sequence using τ_a. The sequence of images contains the interface region between a colloidal crystal and a colloidal liquid. The colloidal crystal is located on the left portion of the images and the colloidal liquid is located on the right portion of the images with a roughly vertical interface in between. The crystal/liquid interface is defined by the transition from ordered spheres to disordered spheres.

The analysis was conducted as follows. First, two of the authors made a manual determination of the interface location for each image in the series by tracing a line over where they believed the interface was located. Second, the images were given to three independent experts who also made manual determinations of the interface location for each image in the same manner. Third, the images were analyzed by the machine vision technique described earlier in this paper, which generates an automated determination of the interface location in each image. Figure 10 shows the first, fifth, and tenth images analyzed by the automated interface technique. Figure 11 shows the average of the authors' interface locations compared to the automated interface technique. Figure 12 shows the average of the experts' interface locations compared to the automated interface technique. For comparison purposes, when using a human observer's determination of the interface location, the midpoint of the traced line was taken.

Table 1 shows the comparative analysis of image stability using the first image in each sequence as a baseline. The data shows that the automated interface technique has the smallest position change on average by a factor of 2 to 5 compared to the manual results. For each image, the distance from a given human observer's interface to the automated interface was found simply by taking the distance for each row of the image and averaging. The comparative analysis between our automated interface technique calculations and the authors' manual calculations is listed in table 2. The comparative analysis between our automated interface technique calculations and the independent experts' manual calculations and the data is listed in table 3.

Discussion

The main finding of this research is that the automated interface algorithm appears to be more reliable at identifying the transition zones in our microscopy images than the human experts. Theoretically, there should not be a significant difference in the interface location over the course of the image sequences shown in figures 9 through 12 as a result of the slow growth velocity and short time duration chosen, so for each method (whether automated or human), the perceived interface location should remain stable. The human observers were tested for reliability by finding the distance between the interface location in each image as compared to the first image. The same was done for the automated technique.

Using the authors' manual data, the average interface pixel difference from the automated interface technique was 9.2 pixels. Using the independent experts' manual data, the average interface pixel difference from the interface technique was 10.9 pixels. As can be seen in figures 11 and 12, the largest variations occurred for the crystal grain closest to the bottom of the image. However, the largest variations between manual results also occurred within this region. This seems to indicate that the interpretation of the interface position is more ambiguous for this particular crystal orientation for both human observers and our computer algorithm alike. However, the overall agreement between manual and automated results is quite good. The sphere diameter in our images was 7.1 pixels, so the average variation from author and independent expert results were 1.3 and 1.5 particle diameters, respectively. Therefore, the average variation between the automated and manual interfaces was at most only one-half the dimension of the theoretical interface width, which is predicted to be approximately 3 to 7 particle diameters wide (Curtain, 1989; Chowhury and Ghosh, 1998).

We found that the interface calculated by our algorithm deviated from the manual results by only about one-half the theoretical width of the transition region, and the repeatability of the algorithm results was better than that of the manual results. Experiments that would take weeks or even months to analyze manually can now be done in a matter of minutes or hours using our automated interface detection technique. The interface detection technique described in this paper is directly applicable to any imaging application where regions of interest are distinguished from the background by differing patterns of motion over time.

References

Bethea, M.D. 1996. High Precision Algorithms for Stereo Imaging Velocimetry, Ph.D. Dissertation. Department of Computer Engineering and Science, Case Western Reserve University.

Bogomolov, V.N., Gaponenko, S.V., Germanenko, I.N., Kapitonov, A.M., Petrov, E.P., N.V. Gaponenko, N.V., Prokofiev, A.V., Ponyavina, A.N., Silvanovich, N.I. and Samoilovich, S.M. 1997. Photonic band gap phenomenon and optical properties of artificial opals. *Phys. Rev. E 55*, p. 7619.

Choudhury, N., and S.K. Ghosh. "Modified weighted density-functional approach to the crystal-melt interface." *Phys. Rev. E 57*, no. 2 (1998): 1939–1945.

Crouser, P.D., Bethea, M.D., and Merat, F.L. 1997. Unattenuated tracer particle extraction through time-averaged, background image subtraction with outlier rejection. Experiments in Fluids, 22.

Curtain, W.A. 1989. Density-functional theory of crystal-melt interfaces. *Phys. Rev. B 39*, 6775.

Elliot, M.S., Bristol, B.T.F. and Poon, W.C.K. 1997. Direct measurement of stacking disorder in hard-sphere colloidal crystals. *Physica A*, 235, 216.

Gasser, U., Weeks, E.R., Schofield, A., Pusey, P.N. and Weitz, D.A. 2001. Real-space imaging of nucleation and growth in colloidal crystallization. *Science* 292, 258.

Grier, D.G. and Murray, C.A. 1994. The microscopic dynamics of freezing in supercooled fluids. *J. Chem. Phys.* 100 [12], 9088.

McDowell, M. 2003. Stereo Imaging Velocimetry, US Patent no. 6, 603, 535.

Phan, S.E., Russel, W.B., Cheng, Z., Zhu, J., Chaikin, P.M., Dunsmuir, J.H. and Ottewill, R.H. 1996. Phase transition, equation of state, and limiting shear viscosities of hard sphere dispersions. *Phys. Rev. E 54* [6], 6633.

Poon, W.C.K. and Pusey, P.N. "Phase transition of spherical colloids. 1995. Observation, Prediction and Simulation of Phase Transitions in Complex Fluids, ed. M. Baus et al., 3–51. Kluwer Academic Publishers, Netherlands.

Pusey, P.N. and van Megen, W. 1986. Phase behavior of concentrated suspensions of nearly hard colloidal spheres. *Nature* 320, 340–342.

Subramania, G., Constant, K., Biswas, R., Sigalas, M.M. and Ho K.M. 1999. Optical photonic crystals fabricated from colloidal systems. App. Phys. Lett. 74, p. 3933.

Wijnhoven, J.E.G.J and Vos, W.L. 1998. Preparation of Photonic Crystals Made of Air Spheres in Titania Science, 281, p. 802.

Zakhidov, A.A., Baughman, R.H., Iqbal, Z., Cui, C.X., Khayrullin, I., Dantas, S.O., Marti, J. and Ralchenko, V.G. 1998. Carbon structures with three-dimensional periodicity at optical wavelengths. Science, 282, p. 897.

TABLE 1.—COMPARATIVE ANALYSIS OF INTERFACE STABILITY USING IMAGE 1 AS A BASELINE
(IN PIXELS)

	D1–D2	D1–D3	D1–D4	D1–D5	D1–D6	D1–D7	D1–D8	D1–D9	D1–D10	AVG.
Auto Interface Technique	0.93	1.19	1.4	1.36	1.7	2.19	2.52	3.19	3.64	2.01
Author 1	7.45	5.07	10.61	4.71	4.56	6.47	4.84	3.95	6.81	6.05
Author 2	5.92	3.03	4.93	4.35	3.07	3.57	3.83	3.1	5.9	4.19
									Author Avg.	5.12
Expert 1	8.86	8.82	9.48	13.81	9.48	12.72	8.46	6.92	20.82	11.04
Expert 2	7.87	12.27	7.56	9.38	8.73	9.41	6.89	8.26	8.51	8.76
Expert 3	3.74	8.48	4.81	7.89	6.65	7.3	4.29	7.14	5.61	6.21
									Expert Avg.	8.67

TABLE 2.—AUTHORS' CALCULATED DISTANCE FROM THE
AUTOMATED TECHNIQUE INTERFACE LOCATION

Interface no.	Author 1 (in pixels)	Author 2 (in pixels)	Averaged (in pixels)
1	6.4	12.3	9.35
2	7.2	12.3	9.75
3	7.1	10.0	8.55
4	7.4	12.7	10.05
5	6.7	11.2	8.95
6	7.0	11.6	9.3
7	6.1	9.4	7.75
8	7.7	9.7	8.7
9	7.4	12.1	9.75
10	7.1	11.6	9.35
Average	7.01	11.29	9.15

TABLE 3.—EXPERTS' CALCULATED DISTANCE FROM THE
AUTOMATED TECHNIQUE INTERFACE LOCATION

Interface no.	Expert 1 (in pixels)	Expert 2 (in pixels)	Expert 3 (in pixels)	Averaged (in pixels)
1	13.5	13.6	11.30	12.80
2	15.1	10.8	11.70	12.53
3	17.6	10	8.60	12.07
4	11.3	13	10.00	11.43
5	8.3	10.4	6.90	8.53
6	10.7	10.8	10.00	10.50
7	5.7	8.2	7.20	7.03
8	12.5	11.7	11.00	11.73
9	13.8	12.3	6.50	10.87
10	13.8	10.6	11.20	11.87
Average	12.23	11.14	9.44	10.94
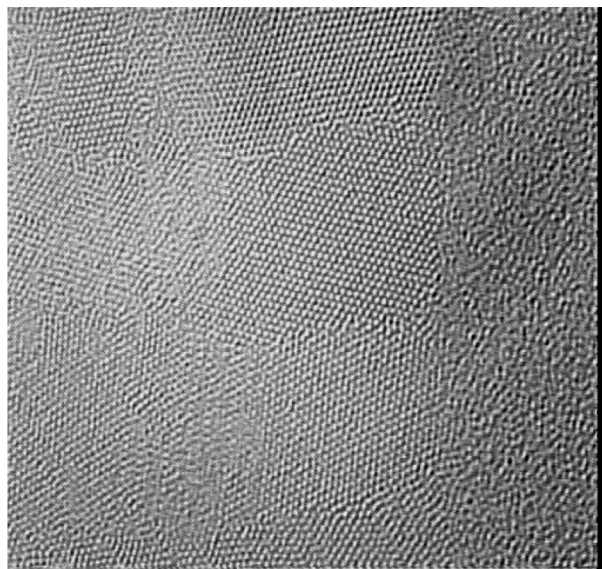
Figure 1.—Typical colloid image.
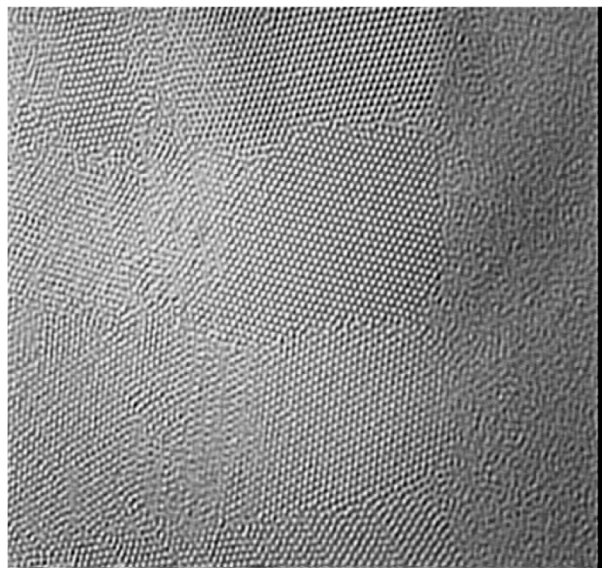
Figure 2.—Frame-averaged image (n = 10).
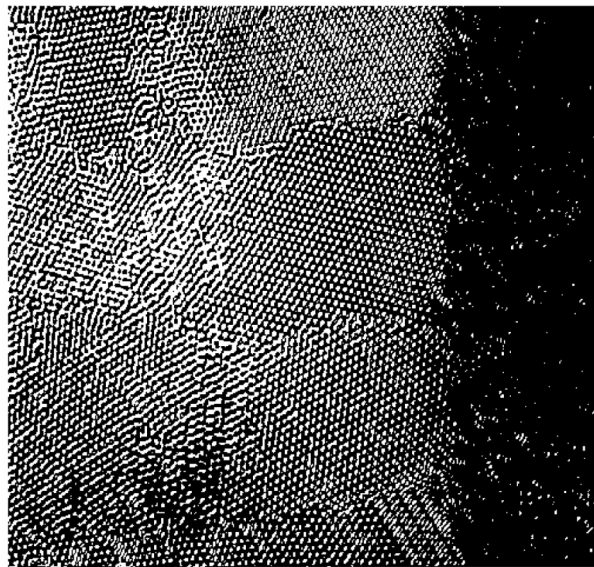
Figure 3.—Result of brightness slicing on a frame-averaged image (n = 10).
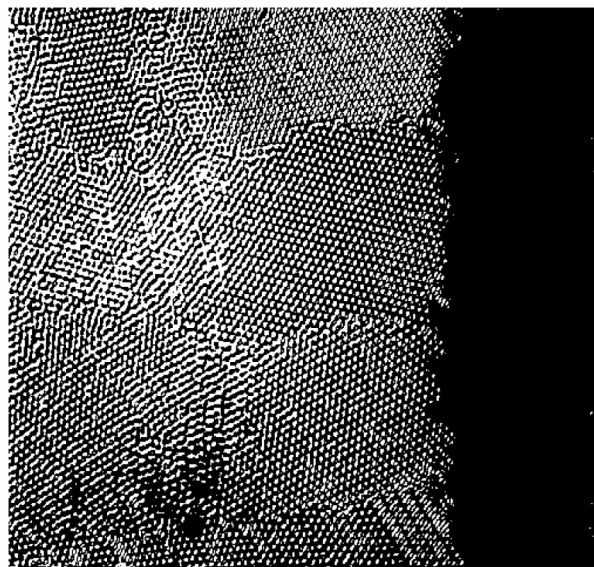
Figure 4.—Result of clean technique (n = 10).
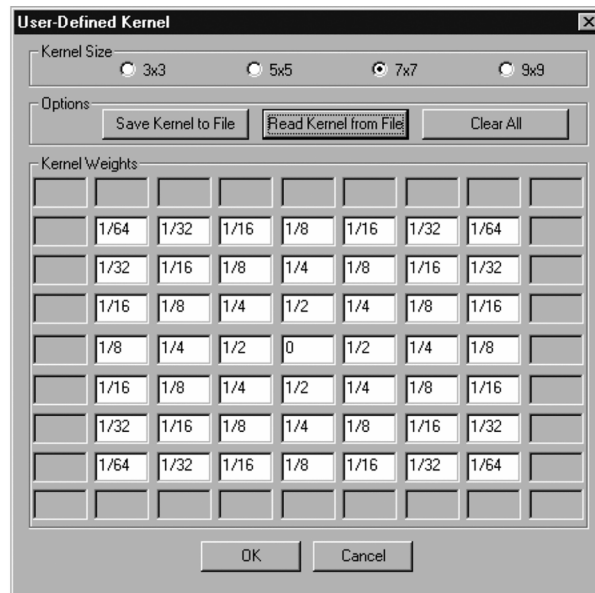
Figure 5.—Low pass filter weights.
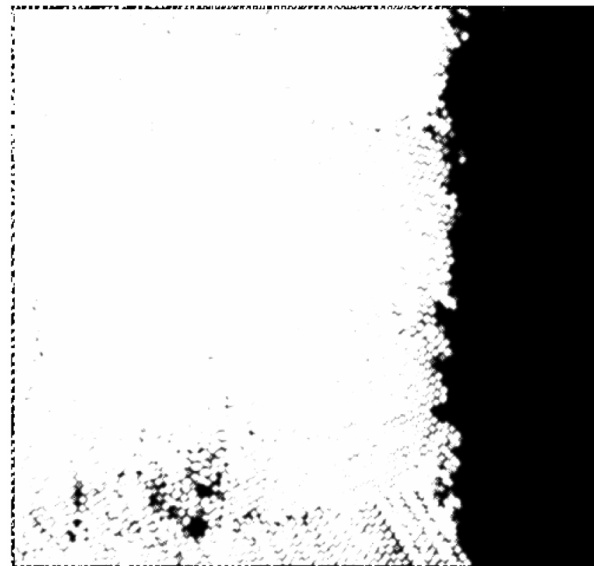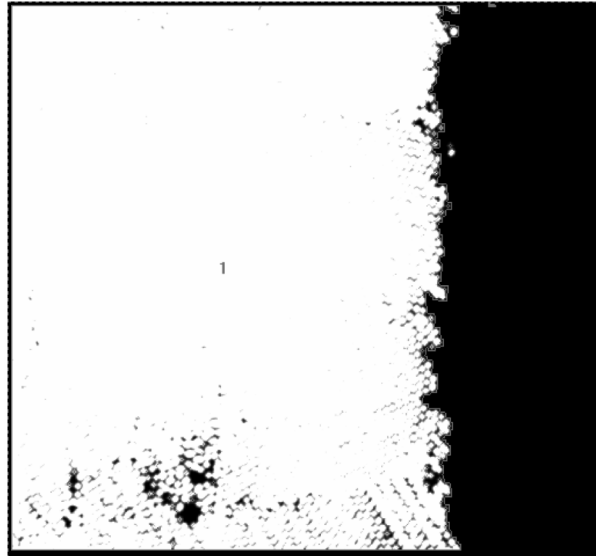

Figure 6.—Result of image dilation (n = 10).
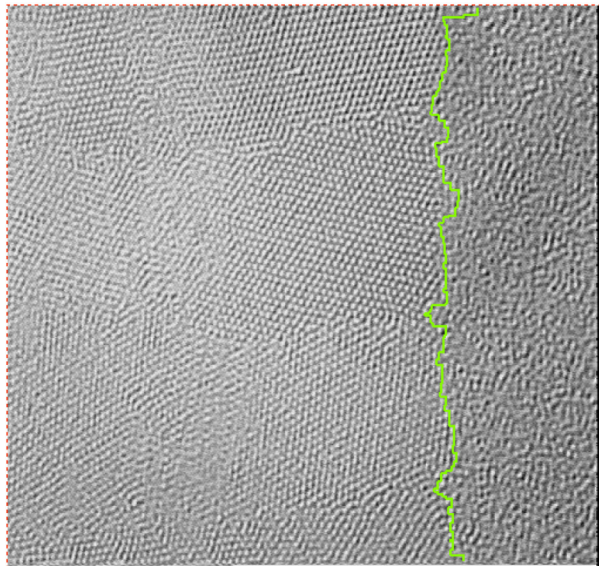
Figure 7.—Result of find particles technique (n = 10).

Figure 8.—Result of automated interface solution high-
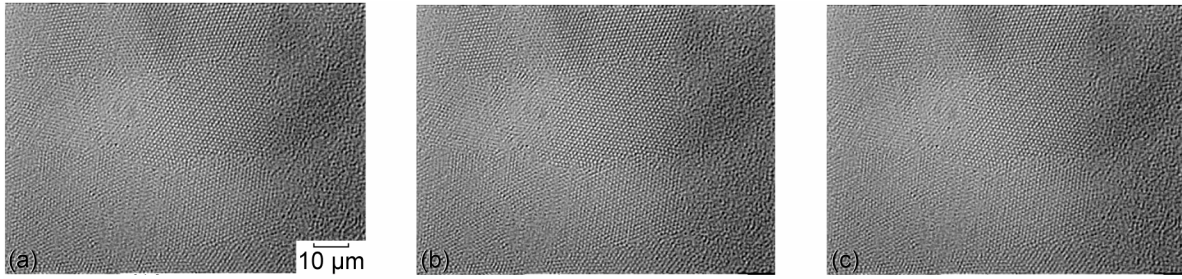lighting solid/liquid interface.

Figure 9.—1st, 5th, and 10th images in the experiment sequence. (a) 1st image. (b) 5th image. (c) 10th image.
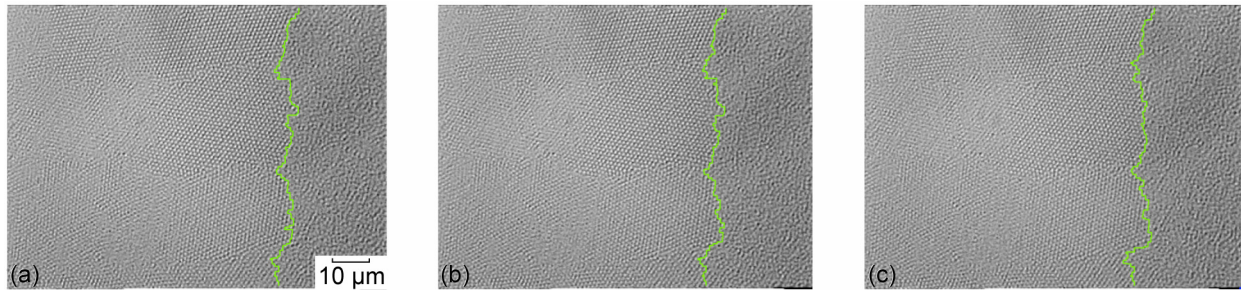
Figure 10.—1st, 5th, and 10th automated interface technique (n = 10) result superimposed on original image. (a) 1st image. (b) 5th image. (c) 10th image.
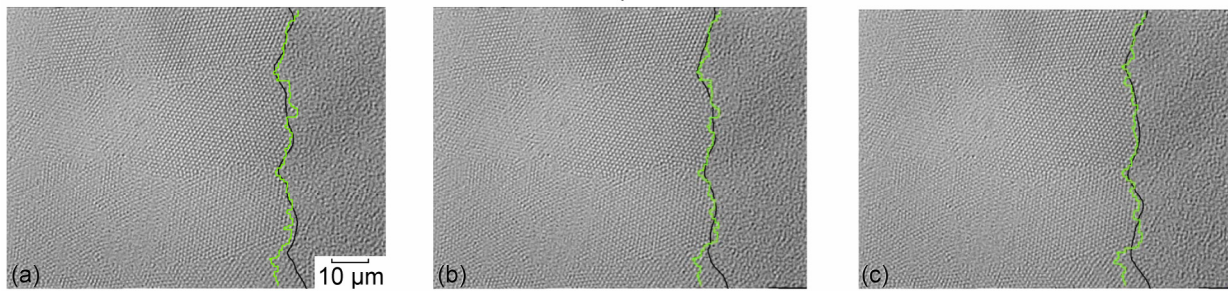
Figure 11.—1st, 5th, and 10th automated interface technique (n = 10) and authors' results superimposed on original image. (a) 1st image. (b) 5th image. (c) 10th image.
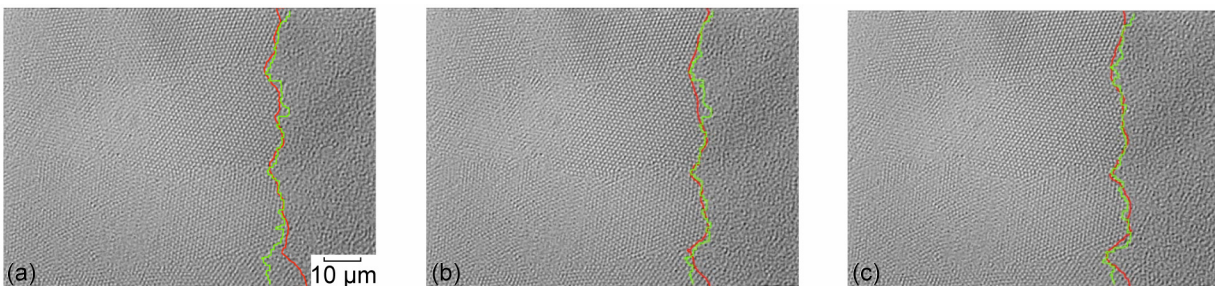

Figure 12.—1st, 5th, and 10th automated interface technique (n = 10) and independent experts' results superimposed on original image. (a) 1st image. (b) 5th image. (c) 10th image.

REPORT DOCUMENTATION PAGE

1. AGENCY USE ONLY (Leave blank)	2. REPORT DATE	3. REPORT TYPE AND DATES COVERED
	October 2005	Technical Memorandum

4. TITLE AND SUBTITLE

An Automatic Phase-Change Detection Technique for Colloidal Hard Sphere Suspensions

5. FUNDING NUMBERS

WBS–22–708–24–05

6. AUTHOR(S)

Mark McDowell, Elizabeth Gray, and Richard B. Rogers

7. PERFORMING ORGANIZATION NAME(S) AND ADDRESS(ES)

National Aeronautics and Space Administration
John H. Glenn Research Center at Lewis Field
Cleveland, Ohio 44135–3191

8. PERFORMING ORGANIZATION REPORT NUMBER

E–15313

9. SPONSORING/MONITORING AGENCY NAME(S) AND ADDRESS(ES)

National Aeronautics and Space Administration
Washington, DC 20546–0001

10. SPONSORING/MONITORING AGENCY REPORT NUMBER

NASA TM—2005-213989

11. SUPPLEMENTARY NOTES

Mark McDowell and Richard B. Rogers, NASA Glenn Research Center; and Elizabeth Gray, Scientific Consulting, Inc., 17418 Puritas Avenue, Cleveland, Ohio 44135. Responsible person, Mark McDowell, organization code RUB, 216–433–8161.

12a. DISTRIBUTION/AVAILABILITY STATEMENT

Unclassified - Unlimited
Subject Categories: 55, 52, and 51

Available electronically at http://gltrs.grc.nasa.gov
This publication is available from the NASA Center for AeroSpace Information, 301–621–0390.

12b. DISTRIBUTION CODE

13. ABSTRACT (Maximum 200 words)

Colloidal suspensions of monodisperse spheres are used as physical models of thermodynamic phase transitions and as precursors to photonic band gap materials. However, current image analysis techniques are not able to distinguish between densely packed phases within conventional microscope images, which are mainly characterized by degrees of randomness or order with similar grayscale value properties. Current techniques for identifying the phase boundaries involve manually identifying the phase transitions, which is very tedious and time consuming. We have developed an intelligent machine vision technique that automatically identifies colloidal phase boundaries. The algorithm utilizes intelligent image processing techniques that accurately identify and track phase changes vertically or horizontally for a sequence of colloidal hard sphere suspension images. This technique is readily adaptable to any imaging application where regions of interest are distinguished from the background by differing patterns of motion over time.

14. SUBJECT TERMS

Image analysis; Image techniques; Pattern recognition; Microscopy; Transition mapping; Automated interface detection; Machine vision

15. NUMBER OF PAGES

20

16. PRICE CODE

17. SECURITY CLASSIFICATION OF REPORT	18. SECURITY CLASSIFICATION OF THIS PAGE	19. SECURITY CLASSIFICATION OF ABSTRACT	20. LIMITATION OF ABSTRACT
Unclassified	Unclassified	Unclassified	